Femtosecond real-time probing of reactions. I. The technique

Mark J. Rosker, Marcos Dantus, and Ahmed H. Zewail

Citation: The Journal of Chemical Physics **89**, 6113 (1988); doi: 10.1063/1.455427
View online: http://dx.doi.org/10.1063/1.455427
View Table of Contents: http://scitation.aip.org/content/aip/journal/jcp/89/10?ver=pdfcov
Published by the AIP Publishing

Femtosecond real-time probing of reactions. I. The technique

Mark J. Rosker, Marcos Dantus, and Ahmed H. Zewail[a)]
Arthur Amos Noyes Laboratory of Chemical Physics, California Institute of Technology, Pasadena, California 91125

(Received 12 July 1988; accepted 11 August 1988)

When a chemical bond is broken in a direct dissociation reaction, the process is so rapid that it has generally been considered instantaneous and therefore unobservable. But the fragments formed interact with one another for times on the order of 10^{-13} s after the photon has been absorbed. On this time scale the system passes through intermediate transition configurations; the totality of such configurations have been, in the recent literature, designated as "transition states." Femtosecond transition-state spectroscopy (FTS) is a real-time technique for probing chemical reactions. It allows the direct observation of a molecule in the process of falling apart or in the process of formation. In this paper, the first in a series on femtosecond real-time probing of reactions, we examine the technique in detail. The concept of FTS is explored, and the interrelationship between the dynamics of chemical reactions and molecular potential energy surfaces is considered. The experimental method, which requires the generation of spectrally tunable femtosecond optical pulses, is detailed. Illustrative results from FTS experiments for several elementary reactions are presented, and we describe methods for relating these results to the potential energy surface(s).

I. INTRODUCTION

In previous publications from this laboratory,[1-4] the observation in real time of the dynamics of chemical bond breaking in elementary reactions has been reported. This is the first paper in a series in which we present a detailed description of the technique and its application to different reactions and give an account of our earlier reports.

In these experiments, an ultrafast optical pulse (pump) is used to initiate the reaction and establish the zero-of-time. While the molecular bond is in the process of breaking, the fragments interact with one another, and using a second femtosecond optical pulse (probe), the dynamics of bond breaking are observed by measuring the perturbed absorption properties in both time and wavelength (t,λ) of one of the fragments.

Of particular interest are the dynamics of elementary reactions, such as

$$ABC^* \rightarrow [A \cdots BC]^{\ddagger *} \rightarrow A + BC, \qquad (1)$$

because of their fundamental nature; namely, a single chemical bond is broken in such a "half-collision." However, the bond is broken so rapidly that direct measurements have not been previously possible. An estimate of the time length for bond breaking can be made as follows: The terminal velocities of separation of the fragments are typically ~ 1 km s^{-1} ($= 0.01$ Å fs^{-1}). If the bond is considered broken when the fragments are a few times their equilibrium bond length apart (typically, several angstroms), then the time required to break the bond must therefore be of the order of a few hundred femtoseconds. During this time period, the system passes through transition states.

Strictly defined, the *transition state* of a reaction is a "configuration of no return" such that once the system has achieved this critical spatial configuration it will necessarily proceed to form products.[5(a)] This state is usually associated with a barrier along the reaction path, e.g., a saddle point. Like other authors,[5-7] we will use the term "transition states" here to refer not only to the one unique state (saddle point), but rather to all intermediate states along the reaction path sufficiently removed from the reagent and product states so as to be experimentally distinguishable from them. It is precisely this region that defines the dynamics during[6] the half-collision (for dissociation reactions) or full collision (for bimolecular reactions).

Molecular beam, chemiluminsence, and laser methods have been the main source of information for deducing the nature of these dynamics from the post-collision (or half-collision) attributes of the fragments.[5(b)] Recently, progress has been made by several groups[7] in using absorption, emission, scattering, and ion spectroscopy to probe the relevant transition region, as reviewed by Polanyi,[7(a)] Kinsey,[7(b)] and Brooks and Curl.[7(c)] An example of how these time-integrated experiments can be used to obtain model potentials is illustrated by the work of Kinsey's group on methyl iodide and Polanyi's group on sodium iodide.[7] In a more recent experiment from Polanyi's laboratory,[7(d)] the transition species of the reaction H + D_2 was observed, to examine potentials for reactions of the H_3 family. Very high sensitivity of detection is required to compensate for the approximately five orders of magnitude difference between the lifetimes of the transition states and the time scale of the experiment. In general, because the transition states are so short lived, their *time evolution* is unresolved in experiments on long time scales.

To detect transition states in real time, our previous experiments on unimolecular[8] and "oriented" bimolecular reactions,[9] using molecular beam picosecond methods,[10] were inadequate. Even picosecond resolution is insufficient for the direct observation of the transitions states. The improved temporal resolution associated with femtosecond transition-state spectroscopy (FTS) is crucial, because it allows the

[a)] John Simon Guggenheim Foundation Fellow.

measurement of the dynamics of the reaction as they occur, starting from the well-defined zero-of-time.

The FTS technique was first applied[1] to the reaction of ICN:

$$ICN^* \rightarrow [I \cdots CN]^{\ddagger *} \rightarrow I + CN\,, \tag{2}$$

which has been studied previously[11] with subpicosecond pulses to monitor the formation of free CN fragments. More recently, FTS was applied to studies of alkali halide reactions, where trapping resonances of photofragments en route to products were observed.[2,3]

This first paper (I) of the series discusses the technique of FTS, both theoretically and experimentally, and illustrates its use as a probe of reaction dynamics in real time. The application of the FTS technique to the reaction ICN $\rightarrow$I + CN is presented in detail in the second paper (II). In future papers from this laboratory, studies of FTS of alkali halides (MX), methyl iodide, and "oriented" bimolecular reactions,

$$MX^* \rightarrow [M \cdots X]^{\ddagger *} \rightarrow M + X, \tag{3a}$$

$$CH_3I^* \rightarrow [CH_3 \cdots I]^{\ddagger *} \rightarrow CH_3 + I\,, \tag{3b}$$

and

$$H + CO_2 \rightarrow [HOCO]^{\ddagger *} \rightarrow HO + CO \tag{3c}$$

will be presented.

This paper is structured as follows: Sec. II gives an overview of the concept of FTS. The experimental method used in our application of FTS is discussed in Sec. III. In Sec. IV, typical experimental observations are presented. Section V deals with the theory of FTS and the interpretation of results. Finally, we will consider techniques by which the FTS results can be used to obtain the potential energy surfaces (PES).

II. OVERVIEW OF FTS

The dynamics of a dissociation reaction, like all reactions, is governed by the PES. In this section, we introduce FTS through a discussion of the dynamical motion of fragments on the appropriate PES. We adopt a classical mechanical approach, but later (Sec. V), we will extend the discussion to include a quantum mechanical (wave packet) picture of the dynamics.

A. FTS and potential energy surfaces

The potential energy surfaces can be quite complicated, involving, for example, van der Waals wells, avoided level crossings, and resonances. We will initially assume, however, that the PES's for the molecule being studied (say, ABC) are particularly simple, as pictured in Fig. 1. Such PES's are in fact typical of many real molecules undergoing direct bond breaking, and have been invoked to describe theories of photodissociation.[12] We further assume that the only relevant configurational parameter is R, the internuclear separation of the fragments in the center-of-mass frame. That is, the PES's are taken to have no angular dependence, as would be the case for a diatomic molecule. In paper II, we will consider consequences of an angular dependence.

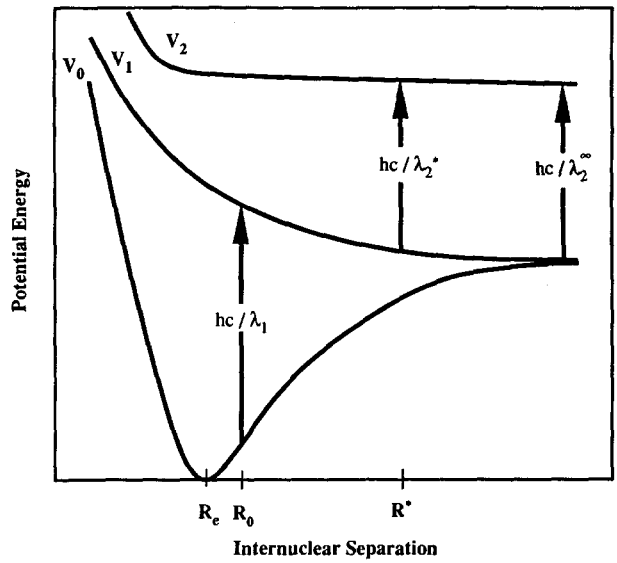

FIG. 1. The PES's of an idealized molecule. V_0 is the PES of the ground state, which has its minimum at $R = R_e$. At time $t = 0$, a pump photon of wavelength λ_1 is absorbed, as indicated by the vertical transition to V_1. The internuclear separation increases as the system evolves on this repulsive potential. At time $t = \tau$, a pulse of wavelength λ_2^* (or λ_2^∞) probes the vertical transition from V_1 to a higher PES, V_2.

Initially, the molecule is in its lowest potential surface V_0. This surface, which represents the bound state of the molecule, will have a well-defined minimum, occurring at an equilibrium internuclear separation R_e.

The FTS experiment begins with an ultrafast optical pulse, with wavelength $\lambda_1 \equiv \lambda_{\text{pump}}$, which initiates the reaction. As a rule, we take all times to be relative to the temporal midpoint of this pump pulse (the "zero-of-time"). The initial internuclear separation R_0 is defined as the distance between the fragments at $t = 0$. In general, $R_0 \neq R_e$, but the excursion of the molecule within the potential well typically will not be great.

Absorption of a photon involves the instantaneous, vertical transition of the molecule from a lower lying PES (in this case, V_0) to an excited PES (here, V_1). The absorption of the photon is appreciable only if at R_0 the difference in the potentials of the two surfaces is nearly equal to the energy of the pump photon,

$$V_1(R_0) - V_0(R_0) \approx hc/\lambda_1\,. \tag{4}$$

The excited molecules prepared by the pump pulse at $t = 0$ will evolve for $t > 0$. The subsequent time evolution of the system wave packet is entirely determined by the details of the excited-state PES. Classically, the molecule falls down V_1, with $R \rightarrow \infty$ as $t \rightarrow \infty$. After the molecule is allowed to evolve for some time delay, $t = \tau$, it is irradiated by the second femtosecond (probe) pulse, with wavelength $\lambda_2 \equiv \lambda_{\text{probe}}$. The probe pulse will only be absorbed if the configuration of the system at time τ is appropriate for a vertical transition from V_1 to a highly excited PES, V_2. Those configurations which allow for absorption of the probe photon are called the optically coupled region (OCR) of the PES by the probe. The OCR will depend on: (1) the *difference* between

the appropriate PES's as a function of the internuclear separation, $V_2(R) - V_1(R)$, and (2) the frequency and spectral width of the the probe pulse.

The FTS signal recorded will be some measure of the absorption by the fragment of the probe pulse as a function of the time delay between pump and probe, τ. This could be accomplished, for instance, by measuring the change in the transmission of the probe. Such an experiment would not be background free; far better sensitivity can be obtained through, for instance, the detection of the laser-induced fluorescence (LIF) or the multiphoton ionization (MPI) generated by the probe. Typically, we measure the FTS signal when λ_2 is tuned to the absorption wavelength of the free fragment, λ_2^{∞} (where ∞ denotes that $R \to \infty$), and at a number of wavelengths absorbed by the transition states, λ_2^{*} (where $*$ denotes the transition-state region of R). Then a surface of measurements $A(t;\lambda_{2(a)}^{*},\lambda_{2(b)}^{*},\ldots,\lambda_2^{\infty})$ is constructed. This surface is related to the dynamics and to the PES of the reaction, as we will discuss below.

B. On-resonant FTS transient: "Clocking"

In the simplest FTS experiment (clocking), the probe is centered at an absorption of one of the free fragments. In this case, the absorption of the probe will be initially negligible, and will only become substantial when the fragments achieve large internuclear distance and are therefore (essentially) noninteracting. The delay at which the probe absorption "turns on," $\tau_{1/2}$, is therefore a direct measurement of the time required for complete (or nearly complete) internuclear separation. In other words, FTS provides a "clock" of the time required to break the bond, and thus, is a fundamental measurement.

The experiment can be pictured simply as a measure of the femtosecond "time-of-flight" on the excited-state PES from the initially excited configuration at R_0 to the free fragment configuration, where the probe opens a "window" on the PES. If the experiment is performed for various probe spectral widths, then additional information on the asymptotic shape of the potential can be collected, as will be further described in Sec. V. Additionally, the clocking experiment offers a significant practical advantage: determination of $\tau_{1/2}$ can be made, in certain cases, to greater accuracy than the temporal width of the pump and probe pulses. The precision to which the time delay can be measured is essentially determined by the experimental signal-to-noise ratio. However, increasing the temporal resolution will eventually lead to further information on the distribution and coherence of molecules as they travel on the PES.

The shape of the FTS transient in the clocking experiment would be an exact step function at $t = \tau_{1/2}$, provided that the following hypothetical conditions held: (1) the pump and probe pulses were delta functions in time and energy, and (2) the wave packet moved on V_1 without dispersion and the intrinsic absorption linewidth was negligible. We now consider the effect of relaxing each of these conditions upon the transient shape. First, assume (for instance) that the intensities of the pump and probe pulses are Gaussian in shape for both frequency and time, with full widths at half-maximum $\Delta\nu$ and Δt, respectively. For transform limited pulses, it will be the case that

$$\Delta\nu\Delta t = 0.44 . \tag{5}$$

Because of the nonzero spectral width of the pump, its OCR on V_1 will actually be a range of R, not a point (namely, R_0); thus, the FTS transient shape is blurred because each molecule will have distinct initial value of R and so will take a different amount of time to reach the probe OCR. Since the pulse energy width is a small fraction of the total available energy, the initial range of R will not be broad, so this effect will generally be less important. As a numerical example, for 100 fs pulses, the spectral width is 150 cm^{-1}, which is to be compared to the total energy of 6000 cm^{-1}, or more. As shown later, however, $\tau_{1/2}$ is directly related to the probe spectral width, since the fragment will clearly take less time to reach the OCR as the window becomes larger.

Of greater effect on the transient shape is the influence of the finite temporal duration of the pump and the probe. The observed FTS transient $A(t)$ will be the convolution of the (ideal) step-function shape with the intensity profiles of both the pump and the probe, which we will call $I_1(t)$ and $I_2(t)$, respectively. We therefore have in this limit (see Appendix)

$$A(t) = \int_{-\infty}^{t} C(x - \tau_{1/2})\, dx , \tag{6}$$

where $C(t)$ is the cross-correlation function of the pump and the probe, given by

$$C(t) = \int_{-\infty}^{\infty} I_1(t - y) I_2(y)\, dy . \tag{7}$$

Aside from the time delay $\tau_{1/2}$, the observed FTS transient is proportional to the response function, which is defined to be the integral of the cross correlation.

In the general case (see the Appendix), the shape of the transient is affected by the wave packet dispersion on the PES. Even classically, each molecule cannot be expected to move uniformly on the excited PES, because the pump pulse will generally prepare a state that may correlate with different vibrational/rotational states, (v, J) of fragment products. Each of the (v, J) states will be associated with different trajectories, and the translational energy of the molecule will be reduced by the vibrational and/or rotational excitation energy. Such trajectories depend on the angular part of the surface, as discussed in paper II.

C. Off-resonant FTS transient: Detuning and transition-states detection

FTS experiments can also be made by tuning λ_2 away from the transition of the free fragment. The final products will thus not absorb the probe, but instead the transition states of the reaction may do so. The FTS transient will therefore be expected to build-up, as the molecules enter the optically coupled region, and then subsequently decay, as the molecules move on to final products. By obtaining FTS transients for various values of λ_2^{*}, i.e., $A(t;\lambda_{2(a)}^{*},\lambda_{2(b)}^{*},\ldots,\lambda_2^{\infty})$, information on the shape of the PES can be obtained.

It is interesting to compare the FTS results obtained in

the off-resonant experiment with those from the on-resonant (clocking) experiment. Since every molecule which enters any given transition state will eventually achieve the final state, the on-resonant FTS transient should be related to an integral of an off-resonant transient. The constant of proportionality here has interesting physical significance, since it is related to both the size of the OCR and the fragment velocity through it, as well as to possible oscillator strength differences. Measurements of $A(t,\lambda_2^*)$ are dependent on the relative changes of the potentials V_1 and V_2 with time.

In cases where the dynamics on V_1 is desired, the probe can be fixed in wavelength, while varying the pump wavelength, i.e., $A(t,\lambda_2^*,\lambda_{1(a)},\lambda_{1(b)},\ldots)$. This way, we change the available energy on V_1. In the center-of-mass frame, we have

$$E = 1/2\mu_{A,BC}v^2 , \tag{8}$$

where v is the terminal recoil velocity of the fragments. Changing the pump wavelength changes v, and thus $\tau_{1/2}$ will decrease in a consistent way, depending on the PES. There is another effect, which may shift $\tau_{1/2}$ in the opposite direction; namely, that as E increases, the travel distance increases. This change in R_0 will generally be small, because of the steep slope of the PES near R_0. (This is shown in more detail in Ref. 13.) From changes in $\tau_{1/2}$ and shapes of the transients, one obtains the dynamics.

D. Femtosecond alignment

To this point, we have discussed the reaction ABC* → A + BC as if its configuration space were one dimensional (with no centrifugal contribution), the only parameter being the distance of A from the center-of-mass of BC. However, the angular part of the potential may be important, and the dynamics may be detected using FTS. As an example, the repulsion of bending ABC will generate a torque during the reaction. This time-dependent angular momentum is related to the alignment, and can be measured by polarization FTS experiments. Transients taken with parallel pump and probe polarizations can be compared with those taken with perpendicular polarizations, as done with time-integrated experiments.[14(a),14(b)] The time dependence of alignment probes two processes. First, the angular part of the potential might lead to different $\tau_{1/2}$'s, depending on the "final" angular momentum state of the BC fragment. Second, the loss of alignment at early times will reflect the degree of the torque which leads to rotations in the BC fragment. Because the BC fragment most probably will be produced in a distribution of angular momentum states, the coherence time[14(c)] is expected to be short, on the order of 50 fs (see paper II and Ref. 37 therein).

III. EXPERIMENTAL APPARATUS

FTS can be applied to a large number of chemical systems. The main experimental difficulty to be overcome is the production of optical pulses of adequate temporal pulse widths (~100 fs or less), wavelengths (typically, in the near ultraviolet), and pulse energy. Additionally, the wavelength of the probe, and in some cases the pump, must be tunable within a set range. Subsequently, the data collection can be accomplished using a variety of techniques; we will discuss two methods we have used in our laboratory. Finally, characterization of the optical pulses and the detection system is crucial. As an example, interpretations of the results can be complicated if a linear frequency chirp of the pump or probe pulses occurs, so that it is important to detect and eliminate such a chirp. In our studies, care is taken to characterize the pulses for every set of data.

A. Pulse generation techniques

In our laboratory, the generation of the optical pulses has been accomplished in four stages (Fig. 2). First, ultrashort pulses were produced at 100 MHz repetition rate near 620 nm by a colliding-pulse mode-locked ring dye laser (CPM), following the pioneering design by Shank and col-

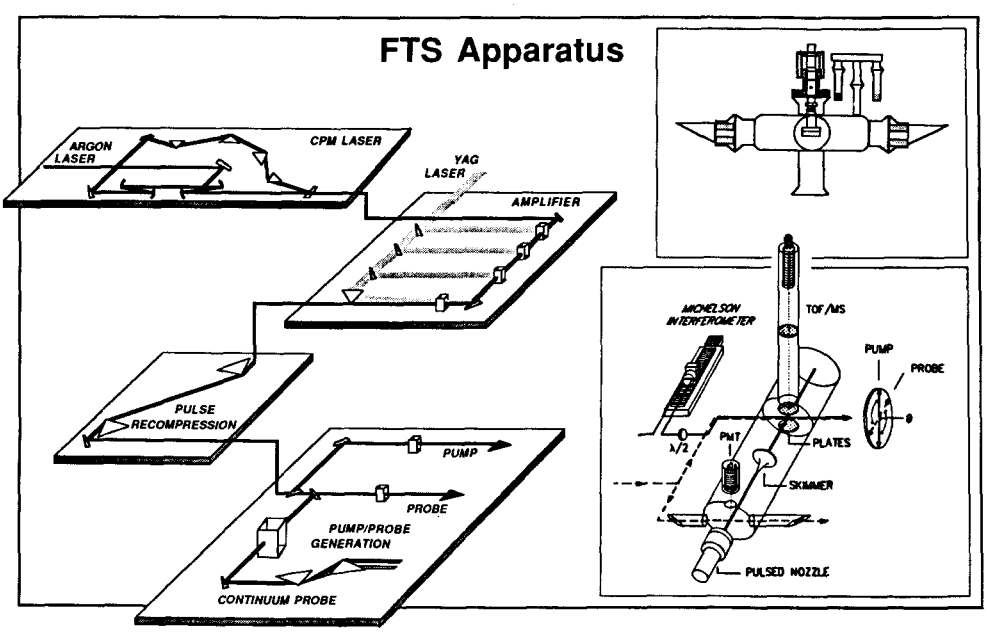

FIG. 2. Overall schematic of the FTS apparatus. The ultrafast pulses are generated in the CPM laser and are amplified in the pulsed dye amplifier. Group velocity dispersion is corrected (recompression) by two prism pairs (only one pair shown). The pump and probe pulses are prepared through a variety of frequency conversion schemes, and are directed into the sample chamber. The chamber is either a gas cell (upper right) or a molecular beam (lower right).

leagues.[15(a)] Although the temporal width of the CPM[15(b)] pulses was sufficient for the experiment, the color and energy were inadequate, so that the pulses were next amplified using a four-stage pulsed dye amplifier (PDA).[15(c)] Third, the large linear frequency chirp of the pulses caused by the group velocity dispersion of the PDA optics was corrected using a prism arrangement. Finally, the appropriate color for the FTS experiment was produced using any of a variety of wavelength conversion schemes.

Our home-built CPM laser [Fig. 3(a)] consisted of seven single-stack dielectric mirrors, arranged to form a ring resonator. Two thin, intracavity jets of organic dyes dissolved in ethylene glycol were positioned near tight beam waists; rhodamine 6G was used to provide the gain and DODCI dye acted as the saturable absorber. The CPM was pumped by 3–4 W of light at 5145 Å by a cw Ar^+ ion laser. Intracavity prisms were used to control the resonator dispersion, thereby affecting pulse widths. With the optimal adjustment of the prisms and the absorber jet, the CPM pulses were measured to be less than 50 fs in duration, using the standard method of autocorrelation by second harmonic generation (SHG) in a nonlinear crystal. These optimal pulses were produced with a central wavelength at 625 nm and with approximately 100 Å bandwidth. For some FTS experiments, the central wavelength of the CPM was continuously tuned to wavelengths as short as 608 nm by suitable adjustment of the intracavity prisms and the saturable absorber jet. When the CPM was tuned in this manner, however, the temporal width of the pulses broadened substantially to as much as ~300 fs (correspondingly, the spectral bandwidth decreased), and a large negative frequency chirp was observed. The chirp was corrected by transiting the output beam through ~15 mm of high density SF10 glass, so that the corrected pulses remained nearly transform limited. An autocorrelation of ~50 fs pulses from our CPM is illustrated in Fig. 4.

The CPM pulses were amplified [Fig. 3(b)] at a 20 Hz repetition rate to 300 μJ energy using a home-built, four-stage, pulsed dye amplifier (PDA). The first three stages of the PDA were transversely pumped, and the fourth stage

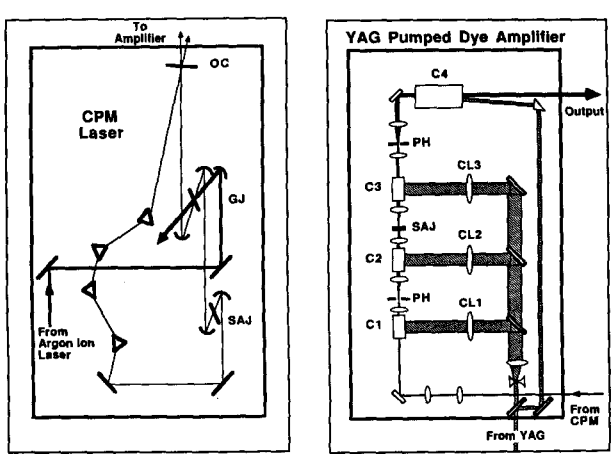

FIG. 3. Schematic of (a) the CPM, and (b) the PDA. Key: SAJ = saturable absorber dye jet; GJ = gain dye jet; OC = output coupler; C1–C4 = dye amplifier cells; CL1–CL3 = cylindrical lenses; PH = pinhole.

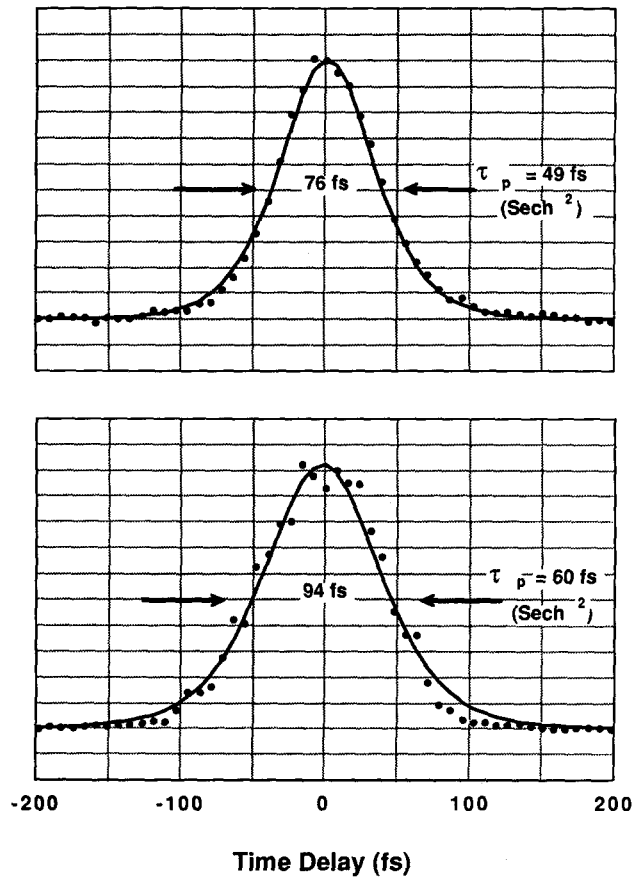

FIG. 4. Typical noncollinear autocorrelation results for the CPM (top) and the PDA (bottom). The solid lines shown are best fits to a sech^2 shape. The full width at half-maximum pulse widths determined from this data are 49 and 60 fs, respectively.

was longitudinally pumped, by the second harmonic of a Nd^{3+}–YAG laser (532 nm). Kiton red in water provided the gain for the first stage, while rhodamine 640 in water was used in the subsequent stages. Using these dyes, the PDA was found to amplify the CPM input throughout its limited tuning range. Amplified stimulated emission (ASE) was suppressed using two techniques: (1) spatial filtering, after the first and third stages, and (2) focusing into a thin jet of a saturable absorber (malachite green dissolved in ethylene glycol), after the second stage.

Because the PDA contained ~150 mm total path length through glass and liquid, broadening of the femtosecond optical pulses by group velocity dispersion was substantial. Nearly perfect recompression of the pulses was accomplished by the suitable arrangement of Fork *et al.*,[16] using four high-index SF10 glass prisms.[17] The advantage of this method over the more commonly used technique with a prism pair is that the prisms were cut to Brewster's angle, and were therefore virtually lossless. Autocorrelation of the recompressed pulses indicated the pulsewidths to be as short as 60 fs, when the CPM was optimized (Fig. 4).

Typically, the pump and probe wavelengths were generated by doubling or by other frequency conversion techniques to produce λ_1 in one arm, and λ_2 in another arm, of a

Michelson interferometer. The relative time delay between the pump and probe beams was set by a microprocessor-controlled linear precision actuator, which adjusted the path length of one arm of the interferometer to submicrometer accuracy. The pump and probe beams, with proper attenuation and with either parallel or perpendicular polarizations, were collinearly recombined by a thin dichroic beam splitter.

The frequency conversion of the PDA light was accomplished through a variety of techniques, depending on the required pump and probe wavelengths and powers. (An example is shown in Fig. 5.) One such technique was second harmonic generation in a thin (500 μm) nonlinear crystal, producing light in the range 304–315 nm. The conversion efficiency measured was > 10%. Another frequency conversion scheme utilized sum frequency generation, whereby excess light from the YAG laser at either 1.064 μm or 532 nm was mixed with the PDA output, also in a phase-matched nonlinear crystal. This approach yielded light in the range 387–396 nm or 284–288 nm, respectively, but the conversion efficiency was limited to a few percent by optical damage of the KD*P crystal. A third technique was the generation with the PDA output of femtosecond white-light continuum pulses.[18] This was accomplished by focusing the 620 nm light into a water cell. At the intensity achieved, nonlinear processes broaden the pulse spectrally (while maintaining its temporal width) to cover an enormous spectral range, from the near UV through the near IR. The appropriate wavelength for the experiment could be selected using an interference filter. Where additional pulse energy was required, a portion of the continuum was amplified in an dye stage pumped by residual 532 nm radiation from the YAG laser. Using these various conversion schemes, probe and pump pulses at the appropriate wavelengths and with 100 nJ to 10 μJ energies were produced.

We have sometimes used these generation techniques in combination (e.g., Fig. 5). For example, for certain experiments (alkali halides[2,3]), broadly tunable pulses near 320 nm were produced by the following scheme: white-light continuum pulses were generated, and directed into an interference filter. This light was amplified to 75 μJ using rhodamine 640 dye. Phase-matched second harmonic generation of this beam yielded the desired optical frequency.

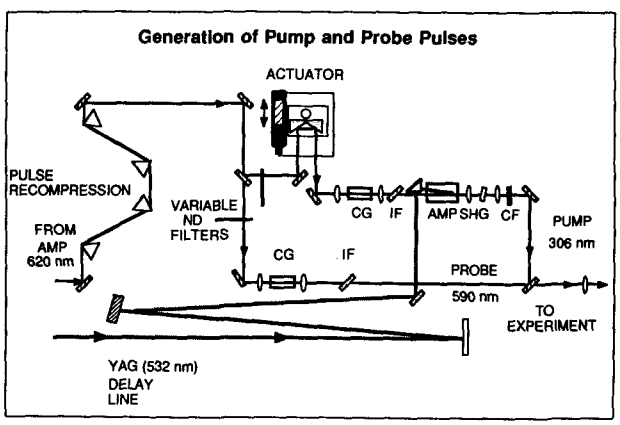

FIG. 5. Schematic of a typical pump/probe generation scheme. One of the many generation schemes used. Key: CG = continuum generation cell; IF = interference filter; SHG = second harmonic generating crystal; CF = color filter; AMP = amplification stage (rhodamine 640).

B. Reaction chamber and data collection

After recombination of the pump and probe, with proper energies and polarizations, the beams were focused through the sample chamber. In many experiments, the sample was a low-pressure gas, in a chamber equipped with LIF detection or MPI signal collection (Fig. 2). For cases where cooling of the initial states is required and/or MPI mass spectrometry is needed,[19] we use a molecular beam, described in detail elsewhere.[8–10] We have recently built as part of our femtosecond apparatus at Caltech a more elaborate molecular beam machine, in order to study reactions of larger molecular systems with FTS.

In the LIF experiments, a lens arrangement was used to collect the fluorescence orthogonal to the direction of the pump/probe pulses. This LIF was dispersed through a 0.34 m monochromator, and detected with a photomultiplier tube. The photomultiplier signal was processed by a boxcar integrator. Care was taken to reject both LIF from multiphoton absorption of the sample by the pump alone (by suitable attenuation of the pump), and scatter of the probe (through the use of baffles, spatial filters, and by temporal gating of the fluorescence). The second detection method used was resonance enhanced multiphoton ionization. In this approach, the probe pulse ionizes one of the fragments, and the ionization current is collected by the application of a dc voltage. Both detection schemes had the crucial advantage of being essentially background free, i.e., the FTS signal ≈ 0 for $\tau < 0$, which increased detection sensitivity. (This would not have been the case, for instance, had the transmitted light been measured.) Furthermore, signal-to-noise was greatly enhanced in both cases by numerically averaging as many as 100 separate data scans for each FTS transient. The experiment was microprocessor controlled, and many diagnostic experiments (e.g., linearity of signal, polarization effects, cross correlation, etc.) were facilitated by such fast data processing methods.

C. Characterization techniques

A variety of diagnostics have been used to characterize the optical pulses and the detection system. These measurements have included: (1) the autocorrelation of the PDA output, (2) the frequency spectrum of the pump and probe pulses, (3) the cross correlation of the pump and probe pulses, and (4) the overall temporal response function of our apparatus including the zero-of-time. Autocorrelation of the 620 nm pulses was made using noncollinear second-harmonic generation in a phase-matched nonlinear crystal. It was insured that the amplifier output (after pulse recompression) was nearly transform limited.

Cross correlation of the pump and probe pulses was complicated by the fact that their colors were generally too blue to allow upconversion in a nonlinear crystal. Instead, the pulse widths were measured by difference frequency gen-

eration of the pump and probe ($\omega = \omega_{\text{pump}} - \omega_{\text{probe}}$), which gave a satisfactory cross correlation.

For the clocking experiments, determination of the exact zero-of-time was crucial, and was accomplished as follows: *In situ*, the molecule studied was evacuated from the chamber and replaced by a molecule which requires both pump and probe photons for photolysis, such as *N,N*-diethylaniline (DEA). The experiment was repeated as before, with the resonance enhanced multiphoton-ionization signal of the DEA measured. It is critical to note that these measurements were made *in situ*, with no re-alignment of the optical beams or re-positioning of the cell, either of which could have significantly shifted the $\tau = 0$. This photoionization experiment gives the integral of the response function of the pump and probe,[11] as we verified by obtaining cross correlation of the pump and probe using nonlinear (IR) difference frequency generation. The zero-of-time was set when the photoionization signal reached one-half its limiting value. Care was taken to insure that pulses were chirp free (transform limited, i.e., $\Delta\nu\Delta t = 0.3$–0.5) for these experiments.

We have also performed a number of check-type experiments to verify our results. For example, it is crucial in clocking experiments to avoid saturation from either the pump or the probe. For each of the experiments, we insured that this was the case both by verifying the linearity of the FTS signal with the power of both the pump and the probe beams, as well as by comparing the transients with those obtained with up to a factor of 10 attenuation of either the pump or the probe. Similarly, we have checked for the effect of scattered light (by changing the gate position and width), effect of gas pressure, polarization of the light, etc.

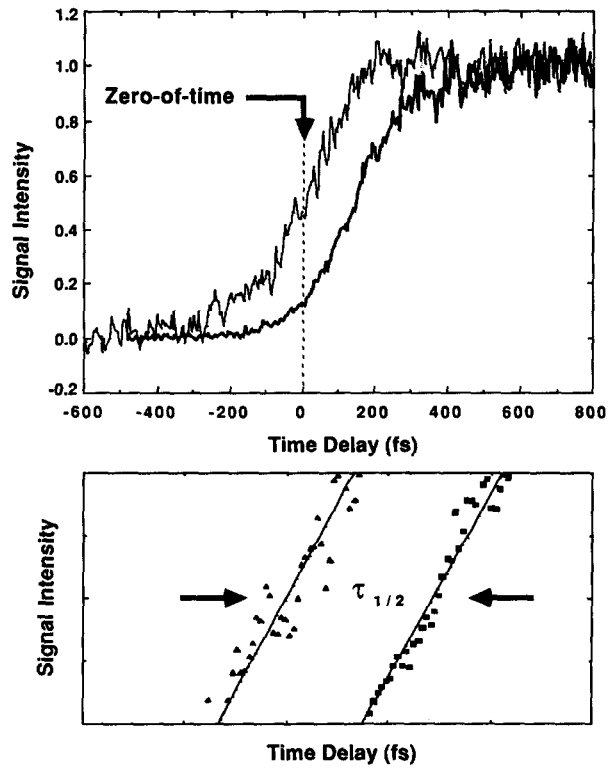

FIG. 6. Typical on-resonant FTS results for the ICN reaction. Top: The thin line is the MPI signal of DEA, which gives the detection-response function and the zero-of-time, as indicated (see text and paper II). The darker line is the FTS data for ICN, taken with $\lambda_2 = \lambda_2^{\infty}$. Note the time delay between these traces, $\tau_{1/2}$. Bottom: The same data, shown on an expanded scale. (See Ref. 4.)

IV. RESULTS

Typical FTS results for the different reactions studied are discussed below. Our focus here is on the applicability of FTS to these reactions, and how in general to relate such observations to the dynamics and to the PES.

A. FTS of the ICN reaction

Iodine cyanide is dissociated following photoexcitation into the $\tilde{A}$ continuum. The PES's of this reaction have been previously considered in detail, both experimentally[20] and theoretically,[21] and are discussed in paper II. There are two relevant channels for dissociation: one corresponding to ground-state iodine (I), and the other to iodine in its excited spin–orbit state (I*). However, for our pump wavelength at $\sim$306 nm, the available energy is insufficient to produce I*, and it is known that the relevant channel is I + CN.

The probe for this experiment was centered at the free-CN transition bandhead at 388.5 nm, or was tuned to the red or to the blue. Results from the on-resonance experiment ($\lambda_2 = \lambda_2^{\infty} = 388.5$ nm) are illustrated in Fig. 6, showing the expected build-up (step-function) behavior, with a $\tau_{1/2}$ delay. The time delay represents the time required to break the molecular bond between the iodine and CN fragments. (See paper II for more details.)

Figure 7 shows typical off-resonant results ($\lambda_2 = \lambda_2^{*}$), which has the expected build-up and decay behavior. Note that for the intermediate cases, the transient decays to some nonzero level, because the spectral width of the probe pulse has a finite value at the on-resonant wavelength. This data reflects the role played by the "window" probe pulse in deducing the properties of the PES, as discussed in paper II, for this reaction. Bernstein and Zewail have used the asymptotic values and shapes of the transients to invert into $\Delta V(t)$.[13] As expected, the peak of the build-up and decay transients (Fig. 7) occurs at earlier times than those of the free-fragment. This follows from the requirement that the fragments enter (and exit) the transition states prior to achieving the final products (see Fig. 1).

B. FTS of alkali halides reactions

The above reaction of ICN involves the dynamics on a repulsive PES. In alkali halide reactions, as evidenced from many molecular beam and spectroscopic studies,[22] the situation is entirely different. Because of the existence of an avoided crossing between the ionic and covalent potential surfaces, the wave packet formed is trapped in a "leaky" potential well, with a certain probability of escape for each encounter which depends on the coupling between the two surfaces. For example, we expect for the reaction of NaI that if the probe wavelength is tuned away from the free-Na absorption at 589 nm, then the "build-up and decay" of the FTS signal, $A(t;\lambda_2^{*})$, will occur not once, but repeatedly.

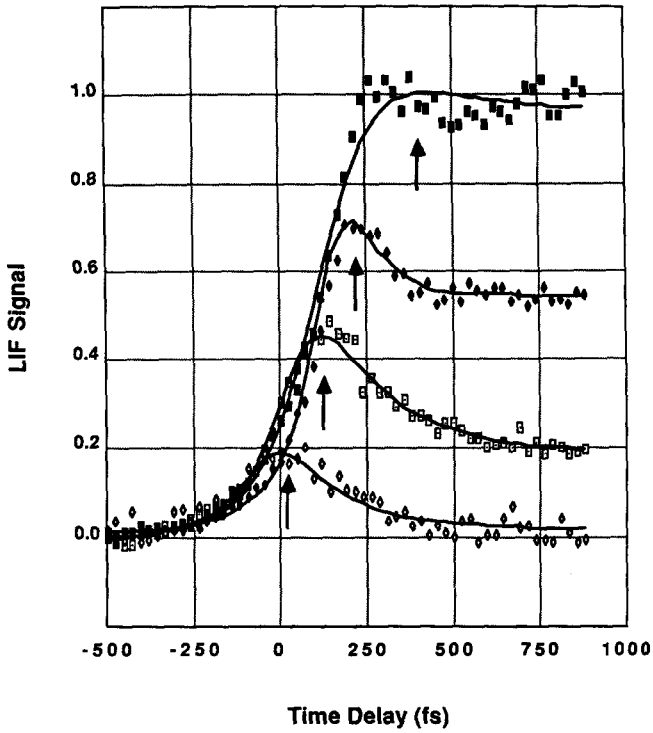

FIG. 7. Typical off-resonant FTS results for the ICN reaction. Key: solid squares: $\lambda_2 = 389.7$ nm; solid diamonds: $\lambda_2 = 389.8$ nm; open squares $\lambda_2 = 390.4$ nm; open diamonds: $\lambda_2 = 391.4$ nm. The zero-of-time is determined separately for each data set using the DEA-MPI technique. The solid lines and arrows are guides to the eye, showing the approximate peak positions for each data set. (Comparison with theory is discussed in more detail in paper II.)

(Note that this behavior would generally be expected, regardless of whether the probe OCR occurred within or outside of the potential well.) On the other hand, if we probe on resonance, $A(t;\lambda_2^{\infty})$, an integrated rise (with plateaus, in this case) is expected.

The FTS transients observed by Rose *et al.* display exactly this sort of oscillatory behavior.[2,3] The repetition rate of the observed FTS maximum is the frequency of the wave packet in the potential well, and the observed damping of the transient gives the escape probability (e.g., the Landau–Zener probability[23]) directly. Varying the wavelength of the pump, $A(t,\lambda_2^{*};\lambda_{1(a)},\lambda_{1(b)},\ldots)$, instead of the probe gives different transients, because the recoil velocity is different, and the dynamics are energy dependent. This was shown in Refs. 2 and 3, where it was used to deduce the anharmonicity of the PES. Wave packet dispersion, discussed previously in the context of the clocking experiments, is also important to the damping of these oscillations.[2,3]

Figure 8, which shows the on-resonant ($\lambda_2 = \lambda_2^{\infty}$) and the off-resonant ($\lambda_2 = \lambda_2^{*}$) NaI FTS results (as well as off-resonant results for NaBr), is a clear demonstration of the concept of FTS. The on-resonant transient rises to a limiting value in a series of plateaus. This is the expected shape, because (as discussed in Sec. II) the on-resonant FTS result should be related to the integral of the off-resonant transient. Thus the plateaus are caused as each of the wave packets of the "train" enter the probe OCR. In transition-state detection, however, oscillations are observed instead, with a frequency which matches perfectly with the separation of the on-resonant plateau steps. More on this analysis will be presented in a forthcoming paper by Rose *et al.*

C. FTS of methyl iodide

We have recently studied the reaction $CH_3I^* \rightarrow CH_3 + I$, where the pump was at 284 nm and the probe at 308 nm. We have recorded FTS transients using multiphoton ionization detection, and a build-up and decay was observed. In this case, we detuned off-resonance to the I fragment to obtain the transients and compare with earlier picosecond MPI mass-spectrometery experiments on CH_3I.[19,24] Work is currently in progress to expand upon these preliminary measurements and to relate these observations to recent theoretical work by Imre and Kinsey[25] and by Shapiro.[26]

V. FROM FTS RESULTS TO THE PES

In the following discussion, we describe the FTS experiments in terms of physical parameters such as the repulsion length parameter of the potential energy surface, the recoil velocity, and the delay time of the fragments. We will use three different approaches to highlight the concepts involved.

A. Kinetic model and FTS sensitivity considerations

We first consider a kinetic approach, which is a heuristic description presented for the sake of illustration and for signal sensitivity considerations. The reaction of ABC passes continuously through transition-state configurations, where the bond stretches from the initial value R_0 to "infinite" sep-

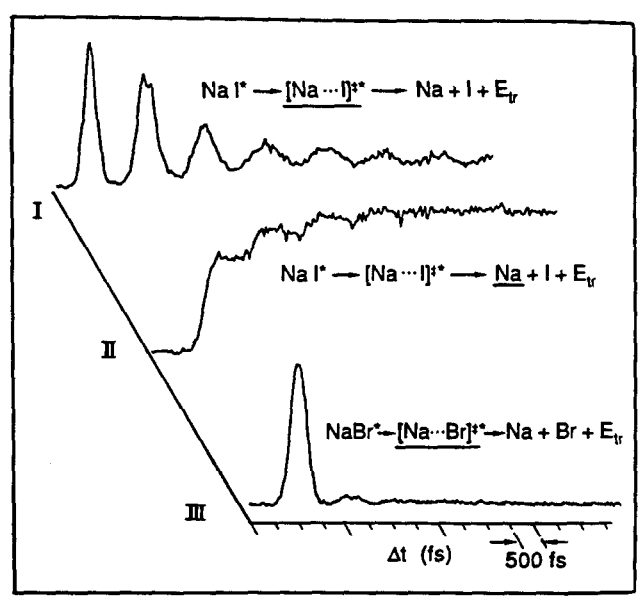

FIG. 8. Typical FTS results for the reactions of NaI and NaBr. (I) transition-state detection for NaI, (II) on-resonance results for NaI, and (III) transition-state detection for NaBr. Note the difference in damping rates in the two reactions, I and III. (See Ref. 2.)

aration. In a simple kinetic model, the continuous nature of the transition states is neglected, and instead the reaction is pictured as passing through a "discrete" number of intermediates. It also cannot describe important features like angular momentum distributions, energy disposal among modes, etc.

The simplest case is the six-level kinetic model diagrammed in Fig. 9, where only one transition state is assumed. An *ad hoc* assumption is made in this case that the rate of population change from one level to another is governed by simple rate equations. These assumptions lead to the following coupled rate equations:

$$\begin{bmatrix} \dot{n}_a \\ \dot{n}_b \\ \dot{n}_c \\ \dot{n}_d \\ \dot{n}_e \\ \dot{n}_f \end{bmatrix} = \begin{bmatrix} -r_1(t) & r_1(t) & 0 & 0 & 0 & 0 \\ r_1(t) & -k_{bc}-r_1(t) & 0 & 0 & 0 & 0 \\ 0 & k_{bc} & -k_{ce}-\beta r_2(t) & \beta r_2(t) & 0 & 0 \\ 0 & 0 & \beta r_2(t) & -k_{df}-\beta r_2(t) & 0 & 0 \\ 0 & 0 & k_{ce} & 0 & -(1-\beta)r_2(t) & (1-\beta)r_2(t) \\ 0 & 0 & 0 & k_{df} & (1-\beta)r_2(t) & -(1-\beta)r_2(t) \end{bmatrix} \begin{bmatrix} n_a \\ n_b \\ n_c \\ n_d \\ n_e \\ n_f \end{bmatrix}, \tag{9}$$

where we make the following definitions:

$n_i(t) \equiv$ the instantaneous population of state $|i\rangle$,

$k_{ij} \equiv$ the rate of spontaneous decay of molecules from state $|i\rangle$ to state $|j\rangle$,

$r_1(t) \equiv$ the instantaneous rate at which the pump pulse excites from state $|a\rangle$ to state $|b\rangle$,

and

$r_2(t) \equiv$ the instantaneous rate at which the probe pulse excites from state $|c\rangle$ to state $|d\rangle$ and from $|e\rangle$ to $|f\rangle$ (see below).

Further, β is defined as a dimensionless parameter describing the relative ratio of the two probe absorptions. Thus, by definition, $\beta = 1$ if the probe is tuned perfectly to the transition-state absorption ($|c\rangle \rightarrow |d\rangle$), whereas $\beta = 0$ if the probe is tuned completely to the final state transition ($|e\rangle \rightarrow |f\rangle$). The rate at which the pump excites the system (from $|a\rangle$ to $|b\rangle$) is given by

$$r_1(t) = I_1(t)\sigma_{ab}\lambda_1/hc\,, \tag{10}$$

and, similarly for the probe,

$$r_2(t) = I_2(t)\sigma_{ef}\lambda_2/hc\,. \tag{11}$$

Here σ_{ij} is the cross section for absorption from $|i\rangle$ to $|j\rangle$, λ_1 and λ_2 are the wavelengths, and $I_1(t)$ and $I_2(t)$ are the intensity profiles of the pump and probe, respectively. We also assumed that the cross section for the on- and off-resonant transitions are equal ($\sigma_{cd} = \sigma_{ef}$). This analysis explicitly takes into account: (1) the finite temporal width of the pump and the probe, (2) stimulated emission, and (3) possible saturation of the transition by the pump and/or the probe.

The above differential equations can be numerically integrated. The appropriate boundary conditions for the problem are given by

$$n_a(-\infty) = N, \tag{12a}$$

$$n_b(-\infty) = \cdots = n_f(-\infty) = 0\,, \tag{12b}$$

where N is the total number of molecules in the sample volume. Figure 10 shows the calculated populations as a function of time for several of these levels. The parameters used are given in the figure caption, and the time scale is expanded to picoseconds to show the behavior at long times. The FTS signal expected from this model would be proportional to $n_f(t)$, the population of the upper final product state. For LIF, as an example, fragments in state $|f\rangle$ will eventually fluoresce and be detected, but they do so on a nanosecond time scale, which is not relevant to the femtosecond dynamics. The results of the numerical integration as a function of the time delay between the pump and probe are presented in Fig. 11.

As witnessed by the similarity of these results with actual data (e.g., Fig. 7), this straightforward approach reproduces the qualitative features observed in the data (at least

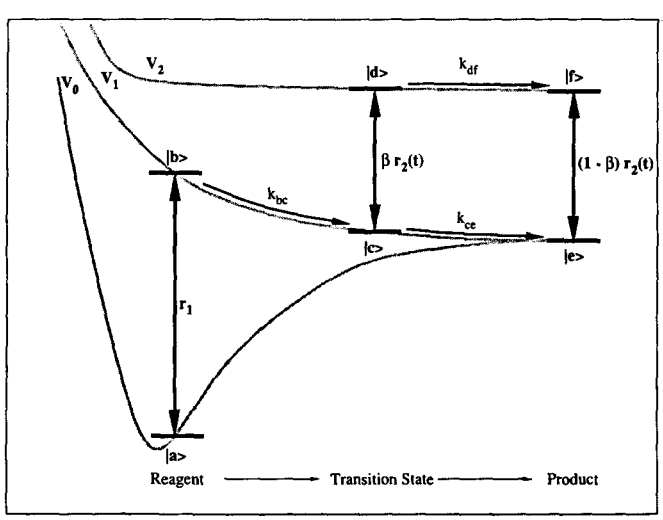

FIG. 9. Schematic of the simple kinetic (six-level) model. The continuum of transition states is described as a single pair ($|c\rangle$, $|d\rangle$) of states. The pumping and probing rates are $r_1(t)$ and $r_2(t)$, respectively. The k_{ij} give the spontaneous transition rates from $|i\rangle$ to $|j\rangle$, as shown. β is defined in the text. Stimulated emission by the pump and probe is indicated by the double headed arrows.

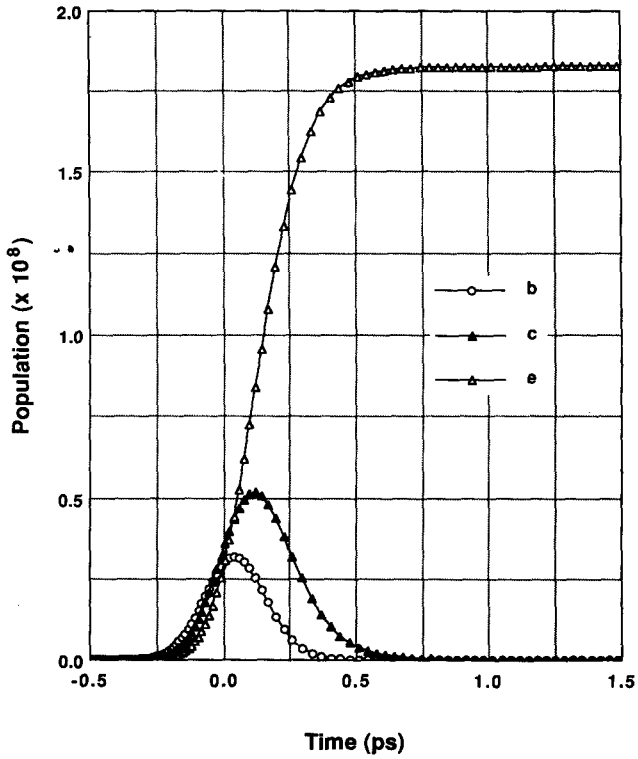

FIG. 10. Population evolution of the simple kinetic model. The instantaneous population of three of the six states are shown as a function of time. Key: open circles $= n_b(t)$, solid triangles $= n_c(t)$, open triangles $= n_e(t)$. Assumed parameters (see the text for definitions): $k_{bc} = 2\times10^{13}\,s^{-1}$, $k_{ce} = k_{df} = 10^{13}\,s^{-1}$, τ (delay time) $= 500$ fs, $N = 10^{12}$ molecules, $\sigma_{ab} = 4\times10^{-20}\,cm^2$, $\sigma_{cd} = 5\times10^{-17}\,cm^2$, and $\beta = 0.95$. In addition, the energies of the pump and probe beams were taken to be 150 and 50 nJ, respectively, with a common width of 150 fs and beam radius of 40 μm. Note that for $\sim$250 fs, the population of the transition state (n_c) is a significant fraction of that of the final state (n_e).

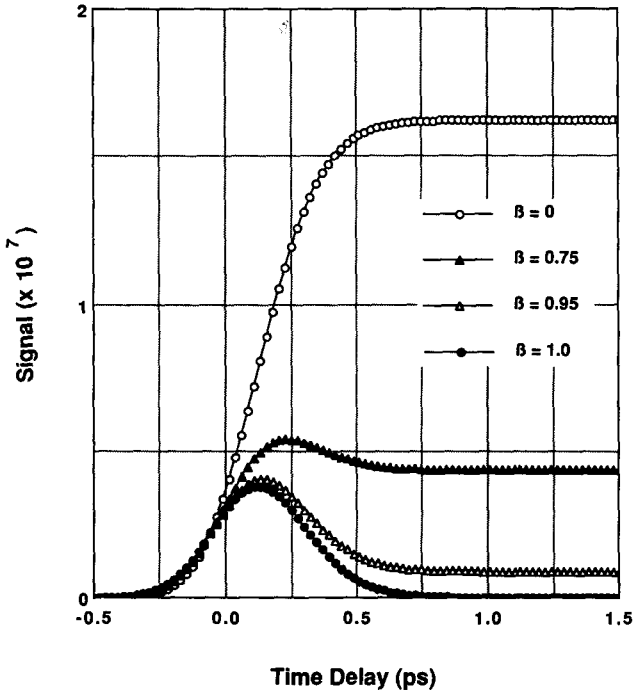

FIG. 11. Predicted FTS results from the simple kinetic model. The signal was calculated using the same parameters as for Fig. 10, as a function of the tuning parameter β. Key: open circles: $\beta = 0$; solid triangles: $\beta = 0.75$; open triangles: $\beta = 0.95$; and solid circles: $\beta = 1.0$. Here, the signal is the population in level $|f\rangle$ (sampled at long times; see Fig. 10) as a function of pump–probe delay time.

for the case of a simple, repulsive potential). The kinetic model duplicates the following experimentally observed FTS behavior: a rise and decay for off-resonant probing, an (integrated) rise to a limiting value for the on-resonant transient, and a linear combination of these shapes for intermediate cases ($0 < \beta < 1$). Some simple points are raised by this analysis. First, it is interesting to note that all of these transient shapes are observed even though the temporal pulse widths assumed in the calculation (150 fs full width at half-maximum, for both pump and probe) is long relative to the assumed kinetic rates ($1/k_{bc} = 50$ fs, and $1/k_{ce} = 1/k_{df} = 100$ fs), suggesting that the transition states can be observed fairly easily with FTS. Second, although the shape of the "intermediate" transients typically observed for ICN can be duplicated using the kinetic model, large values of β are required in the calculation. The physics of β will become more clear as we consider the PES both below and in paper II. It should be noted that the intrinsic linewidth of the final-state transition may be only a small fraction of the spectral width of the probe pulse, but because there are a continuum of transition states, the bandwidth of the (aggregate) TS absorptions may be proportionally much higher. Third, this analysis has indicated that the inclusion at high intensity of stimulated emission in the calculation does not introduce additional features (e.g., an overshoot) in the transients.

We have used this model to investigate the expected effects of saturation on the FTS transients. In Figs. 12 and 13, predicted FTS results are shown for several values of probe fluence, ranging from the linear regime to complete saturation, for the on-resonant and off-resonant cases, respectively. From these studies, we have concluded that the shape of the FTS transient is not dramatically affected by pump or probe saturation (particularly the former). However, increasing saturation is associated with an overall shift in the transient toward earlier time delays, because the first part of the optical pulse begins to bleach the absorption. The effect of such saturation is particularly deleterious for the clocking experiment, since the measured $\tau_{1/2}$ in the presence of saturation by either the pump or the probe would therefore be erroneously small. The effect of saturation on transition-state detection is to decrease the relative amplitude of the peak, but not to introduce an overshoot where one did not previously exist.

The above simple analysis helps illustrate the sensitivity of FTS. Consider, for example, the population of the transition-state $n_c(t)$. From the kinetic model, taking the same parameters as for Fig. 10, the maximum value of $n_c(t)$ is 5.2×10^7 molecules, which is achieved at $t = 120$ fs after pump excitation. This is to be compared with the limiting value of the product state, $n_e(t)$, which for this case is 1.8×10^8 molecules. Thus, even allowing for the temporal

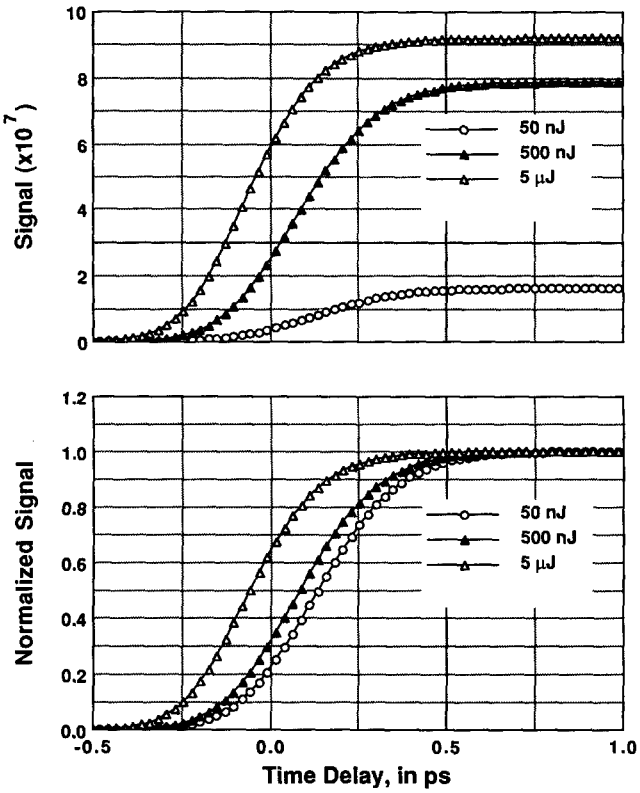

FIG. 12. Effects of probe saturation for the clocking (on-resonant) experiment. The calculation was made using the simple kinetic model. Note the shift in the $\tau_{1/2}$ position, defined to be the time at which the normalized signal reaches 1/2. Key: open circles: probe energy = 50 nJ (linear regime); solid triangles: probe energy = 500 nJ (slight saturation); open triangles: probe energy = 5 μJ (severe saturation). The bottom figure is for the same parameters as the top one, except that the asymptotes are normalized to one.

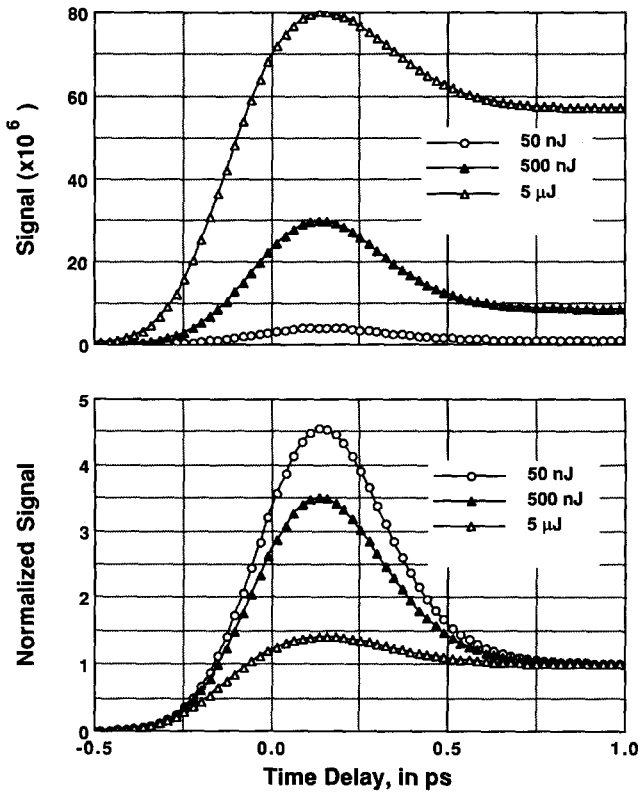

FIG. 13. Effects of probe saturation for the off-resonant experiment. Key: open circles: probe energy = 50 nJ (linear regime); solid triangles: probe energy = 50 nJ (slight saturation); open triangles: probe energy = 5 μJ (severe saturation). The bottom figure is for the same parameters as the top one, except that the asymptotes are normalized to one.

resolution of the optical pulses, the instantaneous population of the transition state which can be probed in an FTS experiment can be as high as 30% of all molecules which will eventually achieve the product state. In comparison, for a "steady-state" (i.e., nanosecond or longer) experiment, the ratio of $n_c(t)/n_e(t)$ would be $\sim 10^{-6}$, because the lifetime of $|c\rangle$ is ultrashort. Thus with FTS, the net enhancement is a million or so.

B. Classical mechanical model

A more descriptive model has been developed by Bersohn and Zewail,[27] who considered the process of bond breaking as a classical motion of the two fragments on the potential surface. Suppose the probe pulse is centered at a wavelength whose absorption is at a maximum for some internuclear separation $R = R^*$. Since the spectral width of the femtosecond pulse in most cases can be expected to exceed the intrinsic linewidth of the transition, the absorption of the probe pulse at an arbitrary value of R is given by

$$A(R) = C/\{\gamma^2 + [\Delta V(R) - \Delta V(R^*)]^2\}, \qquad (13)$$

where γ is the half-width of the optical pulse, $\Delta V(R) \equiv V_2(R) - V_1(R)$, and C is a constant. (Here, the absorption is Lorentzian in shape, but similar expressions could be written for a Gaussian or other shapes.) It is the absorption of the probe as a function of time, $A(t)$, which is directly proportional to the measured signal in an FTS experiment[28]:

$$A(t) = C/\{\gamma^2 + [\Delta V(t) - \Delta V(t^*)]^2\}, \qquad (14)$$

where t^* is defined by the requirement that $R = R^*$ at $t = t^*$.

Suppose for simplicity that the upper excited state potential (V_2) is substantially flatter than the lower potential (V_1).[29] In this case, the absorption reduces to

$$A(t) = C/\{\gamma^2 + [V_1(t) - V_1(t^*)]^2\}. \qquad (15)$$

If a form for $V_1(R)$ is used, then the equation of motion for the fragment can then be integrated to solve for the internuclear distance as a function of time, $R(t)$. Combining the two expressions for $V(R)$ and $R(t)$ together yields the potential of the reaction as a function of time, $V(t)$, so that the absorption expected to be seen in the FTS experiment is known explicitly. Conversely, if we know $A(t)$, then we can deduce $V(t)$ and then $V(R)$.

As an example, suppose that the potential is a repulsive exponential in shape:

$$V_1(R) = V_1^0 \exp\{-R/L_1\} \equiv E \exp\{-(R - R_0)/L_1\}, \qquad (16)$$

where E is the total energy and L_1 is the length parameter of

the potential. For this potential, and using the equation of motion:

$$E = 1/2\mu v^2 + V_1(R)\,, \tag{17}$$

one can explicitly relate R and t:

$$R(t) = R_0 - L_1 \ln\left[\operatorname{sech}^2\left\{\frac{vt}{2L_1}\right\}\right], \tag{18}$$

or, equivalently,

$$\exp\left\{-\frac{R(t)-R_0}{L_1}\right\} = \operatorname{sech}^2\left\{\frac{vt}{2L_1}\right\}, \tag{19a}$$

and, thus,

$$V_1(t) = E\operatorname{sech}^2\left[\frac{vt}{2L_1}\right], \tag{19b}$$

where v is the terminal velocity of the fragments. In Fig. 14, the derived $V_1(R)$, $V_1(t)$ and $R(t)$ are all shown in a construction which illustrates the "trajectory" for dissociation through space–time, and which provides the time and distance scales involved for the PES. The FTS signal will in this case be given by

$$A(t) = \frac{C}{\gamma^2 + W^2(t,t^*)}, \tag{20a}$$

where

$$W(t,t^*) = E\left\{\operatorname{sech}^2\left[\frac{vt}{2L_1}\right] - \operatorname{sech}^2\left[\frac{vt^*}{2L_1}\right]\right\}. \tag{20b}$$

The maximum absorption $A_{\max} = C/\gamma^2$ is achieved when $t = t^*$. The normalized FTS signal is therefore

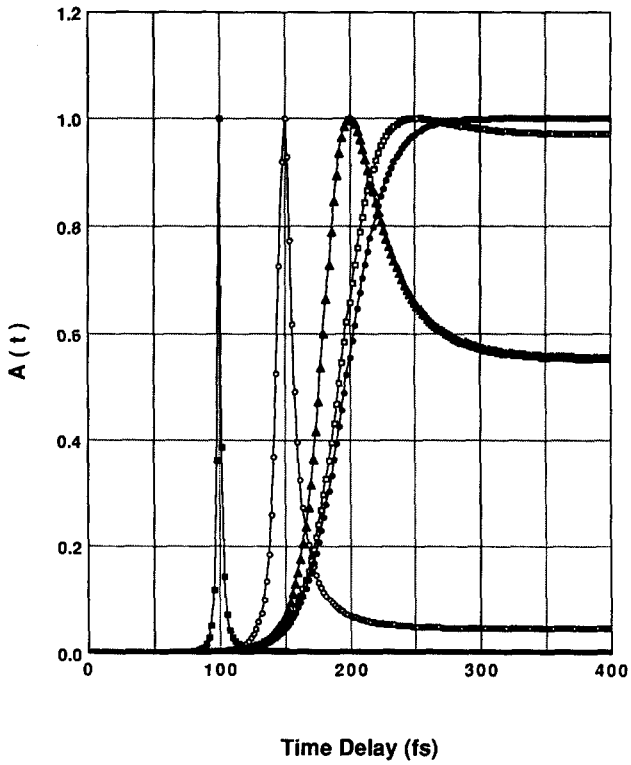

FIG. 15. Predicted FTS results from classical mechanical calculation [Eq. (20)]. Parameters are $L_1 = 0.8$ Å, $v = 0.026$ Å fs^{-1}, $E = 6000$ cm^{-1}, and $\gamma = 40$ cm^{-1} (representative for ICN). The curves shown are for (from left-to-right) $t^* = 100$, 150, 200, 250, and 1000 fs. Note that the peak amplitude of each data set has been normalized to one, and that the calculation does not take into account the finite temporal width of the pulses.

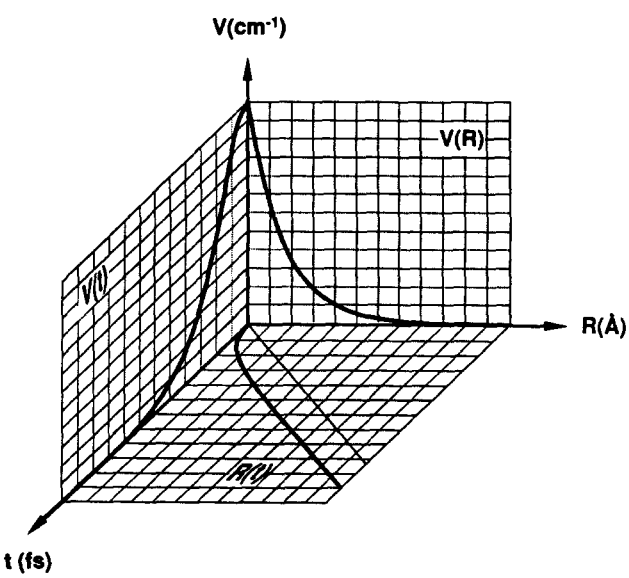

FIG. 14. A potential energy surface as a function of the parameter t (time), with 25 fs per division, and as a function of the parameter R (internuclear distance), with 0.5 Å per division. An exponential shape is assumed and the initial potential energy at $t = 0$ (and $R = 0$) is 6000 cm^{-1} (17.2 kcal/mol above dissociation). Note that the recoil velocity, given by the instantaneous slope of $R(t)$ vs t, rapidly achieves the terminal value. The difference between $R(t)$ and the straight line (which is determined by the terminal velocity) approaches a constant at long time; this difference represents the invariant τ_d defined in the text of paper II.

$$\frac{A(t)}{A_{\max}} = \frac{1}{1 + \gamma^{-2}W^2(t,t^*)}. \tag{20c}$$

This expression is plotted for various values of t^* in Fig. 15. The results reproduce the general features of the observed transients for ICN-type experiments. For $t^* = \infty$, a delayed rise is observed, while for $t^* \neq \infty$, a build-up and decay is deduced. As shown in Ref. 27, the shapes of the transients are entirely determined by the characteristics of the PES.

The results for the clocking experiment can now be modeled by this relation by letting $t^* \to \infty$, so that the probe is centered on the free fragment absorption. The FTS signal will reach half of its limiting value in a time given by

$$\tau_{1/2} = (L_1/v)\ln(4E/\gamma)\,, \tag{21}$$

where E is larger than γ. Thus the FTS data yields in this simple case a direct measurement of the scaling parameter of the potential (L_1). This expression makes explicit an important point raised earlier: the FTS results are affected by the spectral width of the probe pulse (γ), because this determines the optically coupled region of the potential surface. In this case, the probe spectral width determines a window for which the free-fragment LIF is viewed, and so affects $\tau_{1/2}$. With the temporal resolution of FTS experiments, such "dissociation times" must now be carefully defined, as discussed in paper II. According to Eq. (21), $\tau_{1/2}$ is the characteristic dissociation time of the bond, achieved when the potential $V_1(t)$ has dropped to a value of γ. This definition of

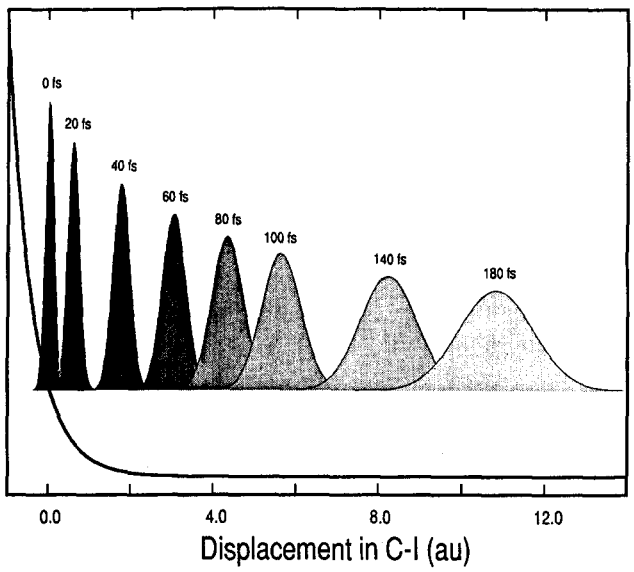

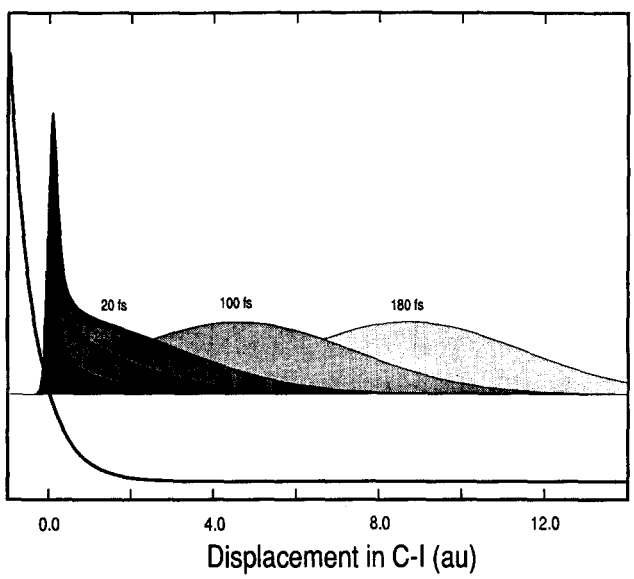

FIG. 16. Wave packet dynamics on an ICN-like PES. The figure shows the evolution of the packet on the first excited state (V_1) for a pump pulse at $\lambda_1 = 306$ nm with (a) a delta-function pulse, and (b) a 125 fs pulse. Reproduced from Ref. 31.

$\tau_{1/2}$ can be verified by comparing the results of Eq. (20c), when $t^* = \infty$ and $t = \tau_{1/2}$, with Eq. (19b).

C. Quantum mechanical model

The problem of molecular bond breaking can also be approached by a quantum mechanical calculation, where the time dependence Schrödinger equation is numerically solved. The wave packet approach of Heller[30] has recently been applied by Williams and Imre,[31] who modeled the FTS experiment for the reaction ICN→I + CN. As above, the dynamics was restricted to one dimension, i.e., the only relevant configurational parameter was the internuclear separation of CN and I. Additionally, an exponential form for both excited potential surfaces (V_1 and V_2) was assumed $\{V(R) = V_0 \exp[-\alpha R] + C\}$, including the amplitudes, length scales, and offsets (V_0, $1/\alpha \equiv L_1$, and C, respectively) for both of these PES's. The calculated wave packet motion on $V_1(R)$ is reproduced in Figs. 16(a) and 16(b), for δ function and 125 fs pulses, respectively.[31]

These results are wonderfully illustrative, because they explicitly show the propagation of the wave packet on the PES, including the packet dispersion. Consistent with our experimental results and with the classical model of the previous section, Williams and Imre predict the form of the transients on and off resonance (Fig. 17). Furthermore, the time scale for the packet movement away from R_0, and spreading is consistent with the experiments.

D. The PES by inversion of FTS data

To this point, we have described the FTS results in terms of model potential surfaces of the reaction. However, a primary purpose of FTS is to obtain information on the shape of the PES's involved. For example, an exponential might approximately describe the PES for a reaction like ICN→I + CN, but such a shape cannot be exact. A repulsive PES will be perturbed by a number of phenomena occurring at long distances, including dipole–quadropole, dipole–induced dipole, and dispersion interactions.

The PES can be reconstructed from the data as follows: In the classical treatment[27] of Sec. V B, the FTS signal obtained was

$$A(t) = C/\{\gamma^2 + [V_1(t) - V_1(t^*)]^2\}, \qquad (22)$$

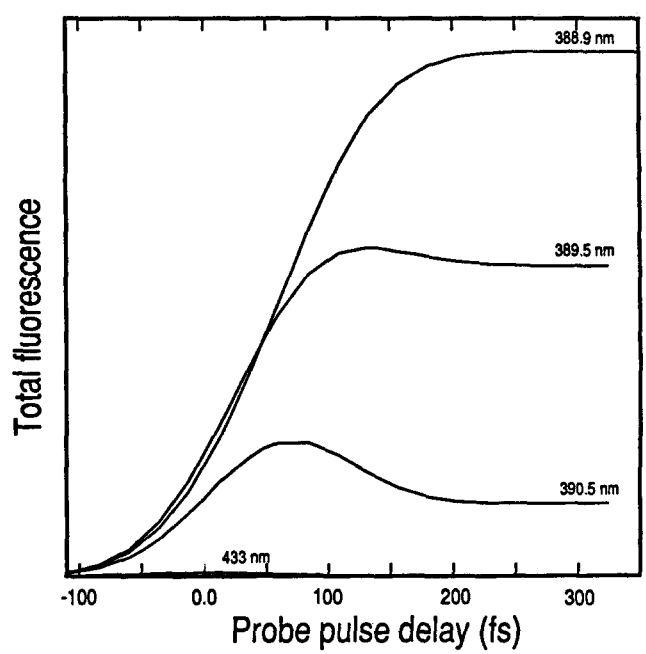

FIG. 17. Predicted FTS results from quantum mechanical calculation. The relative LIF for the indicated probe wavelengths are given for 125 fs pulses. The pump pulse is at $\lambda_1 = 306$ nm. Reproduced from Ref. 31. (See paper II for more discussion of the transients.)

where no assumptions were made as to the form of V_1, but where it was assumed that $V_2(t) - V_2(t^*) \ll V_1(t) - V_1(t^*)$. We can solve the above equation for $V_1(t)$:

$$V_1(t) = V_1(t^*) \pm \gamma \sqrt{\frac{A_{\max}}{A(t)} - 1}\,, \tag{23}$$

where, as before $A_{\max} \equiv C/\gamma^2$. This expression gives the PES directly from the data, but as a function of time. To find $V(R)$, we need to take into account the equation of motion:

$$\frac{dV_1}{dt} = \frac{dV_1}{dR}\frac{dR}{dt} = \frac{dV_1}{dR}\sqrt{\frac{2}{\mu}[E - V_1(R)]}\,. \tag{24}$$

Taken together, the last two expressions can be numerically solved to give $V_1(R)$. Note that at long R, the relationship is rather simple:

$$\frac{dV_1}{dt} = \frac{dV_1}{dR}\cdot v\,. \tag{25}$$

Recently, a more general method[13] has been developed to invert the experimental results and yield quantitative information on the two relevant surfaces involved. Basically, from the shape of the transients in the asymptote (long times) as a function of detuning Δ (defined to be the energy difference between the free fragment absorption and the transition-state absorption), one obtains the absorption probability as a function of the energy window on the potential, i.e., $A(\Delta)$ vs $\Delta V(\Delta)$. By a projection of this experimentally determined shape function on the experimental absorption probability as a function of time, i.e., $A(t)$ vs t, one obtains $\Delta V(t)$ vs t. Repeating the experiments as a function of the pump wavelength and considering the shapes of the transients, as discussed before, should give $V_1(t)$.

In paper II, we apply the classical model to the results on the ICN reaction to obtain $V(t)$ and $V(R)$. In Ref. 13, it is shown how the potential is inverted by the method discussed above. Finally, so far we have not discussed the effect of the angular dependence of the PES, i.e., $V(R,\theta)$, on the observed FTS transients. In paper II, we will address this point, as we show relevant experimental results on the CN-rotational state dependence of FTS transients.

VI. CONCLUSIONS

In this paper, we have considered the experimental and theoretical analysis of FTS. The concept involved was explored, and focus was given to the interrelationship between FTS and the potential energy surface of the reaction. Because of its sensitivity and the time resolution if offers, FTS promises to be successful in probing the dynamics in real time during the "half-collision" of many reactions. Since the recoil velocity of fragments is typically 1 km s^{-1}, the current state-of-the-art in femtosecond generation provides sub-angstrom resolution on the potential. It is our hope to extend these experiments to other classes of reactions, including so called "oriented" bimolecular reactions (full collision), where picosecond studies have already been successful.[9] In the following paper (II), we provide an account of our studies of FTS on the reaction

$$\mathrm{ICN}^* \rightarrow [\mathrm{I}\cdots\mathrm{CN}]^{\ddagger *} \rightarrow \mathrm{I} + \mathrm{CN}\,. \tag{26}$$

ACKNOWLEDGMENTS

This work was supported by AFOSR (Grant No. 87-0071), Contribution No. 7813. During the course of these studies and the development of FTS, we have benefited from fruitful discussions and collaborations with Professor R. Bernstein and Professor R. Bersohn. We also had very helpful discussions with Professor R. Zare, R. Dixon, J. Simons, and K. Wilson on the alignment problem. Finally, we want to thank Dr. T. Rose of our group for helpful discussions, especially relating to his contributions to the work on alkali halides reported in Refs. 2 and 3.

APPENDIX: TRANSIENT SHAPES WITH FINITE WIDTH PULSES

We consider the shape of the FTS transient for the clocking experiment ($t^* = \infty$) when the pump and probe pulses have finite width. First, define the molecular response function $M(t)$ to be the transient shape which would be obtained were the pump and probe pulses infinitely narrow. We will begin by assuming that $M(t)$ is approximately a step function:

$$M(t) = \int_{-\infty}^{t} \delta(x - \tau_{1/2})\,dx\,. \tag{A1}$$

Suppose first that the pump pulse (but not the probe) has appreciable width, and its intensity as a function of time is described by $I_1(t)$. Since each molecule is raised to V_1 at a slightly different time by the pump, the signal would in this case be a convolution of $M(t)$ with $I_1(t)$:

$$[I_1^* M](t) = \int_{-\infty}^{\infty} dy\, I_1(t-y)M(y) \tag{A2}$$

$$= \int_{-\infty}^{\infty} dy \int_{-\infty}^{y} dx\, I_1(t-y)\delta(x - \tau_{1/2}) \tag{A3}$$

$$= \int_{-\infty}^{0} dx \int_{-\infty}^{\infty} dy\, I_1(t-y)\delta(x - \tau_{1/2} + y) \tag{A4}$$

$$= \int_{-\infty}^{t-\tau_{1/2}} dx\, I_1(x)\,. \tag{A5}$$

Since the probe has finite width as well, the observed FTS signal, which we call $A(t)$, will be spread even further, its exact shape given by the convolution of $I_2(t)$ with $[I_1^* M](t)$:

$$A(t) = [I_2^* I_1^* M](t)$$

$$= \int_{-\infty}^{\infty} dy [I_1^* M](t-y) I_2(y) \tag{A6}$$

$$= \int_{-\infty}^{-\tau_{1/2}} dx \int_{-\infty}^{\infty} dy\, I_1(x+t-y) I_2(y)\,. \tag{A7}$$

The cross-correlation function between the pump and the probe intensities can be defined by

$$C(t) = \int_{-\infty}^{\infty} I_1(t-y) I_2(y)\,dy\,. \tag{A8}$$

Substitution into the above relation leads to the conclusion that the observed FTS transient is exactly equal to the inte-

gral of the cross-correlation function, displaced in time by $\tau_{1/2}$:

$$A(t) = \int_{-\infty}^{t} C(x - \tau_{1/2})\, dx\,. \tag{A9}$$

The above result is correct in the limit that $M(t)$ is an ideal step function at $t = \tau_{1/2}$. Generally, if there is a molecular rise, due to, for example, dispersion, then

$$A(t) = [I_2^* I_1^* M\,](t) \tag{A10}$$

$$= \int_{-\infty}^{\infty} dx\, I_2(t-x) \int_{-\infty}^{\infty} dy\, I_1(y) M(x-y)\,. \tag{A11}$$

Equation (A11) will typically be solved numerically.

[1]M. Dantus, M. J. Rosker, and A. H. Zewail, J. Chem. Phys. **87**, 2395 (1987).

[2]T. S. Rose, M. J. Rosker, and A. H. Zewail, J. Chem. Phys. **88**, 6672 (1988).

[3]M. J. Rosker, T. S. Rose, and A. H. Zewail, Chem. Phys. Lett. **146**, 175 (1988).

[4]M. J. Rosker, M. Dantus, and A. H. Zewail, Science **241**, 1200 (1988).

[5]See: (a) R. D. Levine and R. B. Bernstein, *Molecular Reaction Dynamics* (Oxford University, New York, 1974), p. 101; (b) R. D. Levine and R. B. Bernstein, *Molecular Reaction Dynamics and Chemical Reactivity* (Oxford University, New York, 1987), and references therein.

[6]I. W. M. Smith, Nature **328**, 760 (1987).

[7](a) H.-J. Foth, J. C. Polanyi, and H. H. Telle, J. Phys. Chem. **86**, 5027 (1982); (b) D. Imre, J. L. Kinsey, A. Sinha, and J. Krenos, *ibid.* **88**, 3956 (1984); (c) P. R. Brooks, R. F. Curl, and T. C. Maguire, Ber. Bunsenges. Phys. Chem. **86**, 401 (1982); P. R. Brooks, Chem. Rev. **88**, 407 (1988); (d) B. A. Collings, J. C. Polanyi, M. A. Smith, A. Stolow, and A. W. Tarr, Phys. Rev. Lett. **59**, 2551 (1987); (e) R. B. Metz, T. Kitsopoulos, A. Weaver, and D. M. Neumark, J. Chem. Phys. **88**, 1463 (1988); A. Benz and H. Morgner, Mol. Phys. **57**, 319 (1986); (f) J.-C. Nieh and J. J. Valentini, Phys. Rev. Lett. **60**, 519 (1988).

[8]L. R. Khundkar, J. L. Knee, and A. H. Zewail, J. Chem. Phys. **87**, 77 (1987); N. F. Scherer and A. H. Zewail, *ibid.* **87**, 97 (1987); J. L. Knee, L. R. Khundkar, and A. H. Zewail, *ibid.* **87**, 115 (1987).

[9]N. F. Scherer, L. R. Khundkar, R. B. Bernstein, and A. H. Zewail, J. Chem. Phys. **87**, 1451 (1987).

[10]For a recent review, see: J. L. Knee and A. H. Zewail, Spectroscopy **3**, 44 (1988), and references therein.

[11]N. F. Scherer, J. L. Knee, D. D. Smith, and A. H. Zewail, J. Phys. Chem. **89**, 5141 (1985).

[12]See, for example: (a) K. F. Freed and Y. B. Band, in *Excited States*, edited by E. C. Lim (Academic, New York, 1977), Vol. 3, p. 110; (b) M. Shapiro and R. Bersohn, Annu. Rev. Phys. Chem. **33**, 409 (1982); (c) R. Schinke, V. Engel, S. Hennig, K. Weide, and A. Untch, Ber. Bunsenges. Phys. Chem. **92**, 295 (1988).

[13]R. B. Bernstein and A. H. Zewail, J. Chem. Phys. (submitted).

[14](a) See, for example: M. A. O'Halloran, H. Joswig, and R. N. Zare, J. Chem. Phys. **87**, 303 (1987); (b) P. L. Houston, J. Phys. Chem. **91**, 5388 (1987), and references therein; (c) P. M. Felker and A. H. Zewail, J. Chem. Phys. **86**, 2460 (1987).

[15](a) C. V. Shank, Science **233**, 1276 (1986); (b) R. L. Fork, B. I. Greene, and C. V. Shank, Appl. Phys. Lett. **38**, 671 (1981); J. A. Valdmanis, R. L. Fork, and J. P. Gordon, Opt. Lett. **10**, 131 (1985); (c) R. L. Fork, C. V. Shank, and R. T. Yen, Appl. Phys. Lett. **41**, 223 (1982).

[16]R. L. Fork, O. E. Martinez, and J. P. Gordon, Opt. Lett. **9**, 15C (1984).

[17]J. D. Kafka and T. Baer, Postdeadline Report ThZZ5, CLEO '85, Baltimore, May 1985.

[18]R. L. Fork, C. V. Shank, C. Hirlimann, R. Yen, and W. J. Tomlinson, Opt. Lett. **8**, 1 (1983).

[19]L. R. Khundkar and A. H. Zewail, Chem. Phys. Lett. **142**, 426 (1987).

[20]See more details in the following paper [M. Dantus, M. J. Rosker, and A. H. Zewail, J. Chem. Phys. **89**, 6128 (1988)].

[21]See, e.g., E. M. Goldfield, P. L. Houston, and G. S. Ezra, J. Chem. Phys. **84**, 3120 (1986), and references therein.

[22]R. S. Berry, in *Alkali Halide Vapors*, edited by P. Davidovits and D. L. McFadden (Academic, New York, 1979), and references therein.

[23]See, for example, R. B. Bernstein, *Chemical Dynamics via Molecular Beam and Laser Techniques* (Oxford University, Oxford, 1982), p. 168.

[24]J. L. Knee, L. R. Khundkar, and A. H . Zewail, J. Chem. Phys. **83**, 1996 (1985).

[25]R. L. Sundberg, D. Imre, M. O. Hale, J. L. Kinsey, and R. D. Coalson, J. Phys. Chem. **90**, 5001 (1986).

[26]M. Shapiro, J. Phys. Chem. **90**, 3644 (1986).

[27]R. Bersohn and A. H. Zewail, Ber. Bunsenges. Phys. Chem. **92**, 373 (1988).

[28]In this discussion, we neglect the finite width of the pump and probe pulses; strictly speaking, this expression must be convolved with the response function to give the actual FTS signal, as shown in paper II.

[29]To illustrate our point, we take the following condition: $V_2^0 \exp\{-[R(\tau_{1/2}) - R_0]/L_2\} \ll V_1^0 \exp\{-[R(\tau_{1/2}) - R_0]/L_1\} = \gamma$. This can be achieved either by making L_2 less than L_1 or by making $V_2^0 \ll V_1^0$. The use of the more general equation (14) is discussed in Ref. 27 and will be detailed later in a separate study.

[30]E. J. Heller, Acc. Chem. Res. **14**, 368 (1981).

[31]S. O. Williams and D. G. Imre, J. Phys. Chem. (in press).